HHS Public Access

Author manuscript

IEEE Trans Biomed Eng. Author manuscript; available in PMC 2020 August 20.

Published in final edited form as:

IEEE Trans Biomed Eng. 2017 November ; 64(11): 2546–2554. doi:10.1109/TBME.2017.2737559.

Contrast Enhanced Magnetic Resonance Imaging of Gastric Emptying and Motility in Rats

Kun-Han Lu,
School of Electrical and Computer Engineering and Purdue Institute for Integrative Neuroscience, Purdue University, West Lafayette, IN, USA.

Jiayue Cao,
Weldon School of Biomedical Engineering and Purdue Institute for Integrative Neuroscience, Purdue University, West Lafayette, IN, USA.

Steven Oleson,
Weldon School of Biomedical Engineering and Purdue Institute for Integrative Neuroscience, Purdue University, West Lafayette, IN, USA.

Terry L Powley*,
Department of Psychological Sciences and Purdue Institute for Integrative Neuroscience, Purdue University, West Lafayette, IN, USA.

Zhongming Liu* **[Member IEEE]**
Weldon School of Biomedical Engineering, School of Electrical and Computer Engineering, and Purdue Institute for Integrative Neuroscience, Purdue University, West Lafayette, IN, USA.

Abstract

The assessment of gastric emptying and motility in humans and animals typically requires radioactive imaging or invasive measurements. Here, we developed a robust strategy to image and characterize gastric emptying and motility in rats based on contrast-enhanced magnetic resonance imaging (MRI) and computer-assisted image processing. The animals were trained to naturally consume a gadolinium-labeled dietgel while bypassing any need for oral gavage. Following this test meal, the animals were scanned under low-dose anesthesia for high-resolution T1-weighted MRI in 7-Tesla, visualizing the time-varying distribution of the meal with greatly enhanced contrast against non-GI tissues. Such contrast-enhanced images not only depicted the gastric anatomy, but also captured and quantified stomach emptying, intestinal filling, antral contraction, and intestinal absorption with fully-automated image processing. Over four post-ingestion hours, the stomach emptied by 27%, largely attributed to the emptying of the forestomach rather than the corpus and the antrum, and most notable during the first 30 minutes. Stomach emptying was accompanied by intestinal filling for the first 2 hours, while afterwards intestinal absorption was observable as cumulative contrast enhancement in the renal medulla. The antral contraction was captured as a peristaltic wave propagating from the proximal to distal antrum. The frequency, velocity, and amplitude of the antral contraction were on average 6.34±0.07 contractions per minute, 0.67±0.01 mm/s and 30.58±1.03%, respectively. These results demonstrate an optimized

*correspondence powleyt@purdue.edu, zmliu@purdue.edu.

MRI-based strategy to assess gastric emptying and motility in healthy rats, paving the way for using this technique to understand GI diseases, or test new therapeutics in rat models.

Index Terms

magnetic resonance imaging; gastric emptying; gastric motility; antral contraction; image segmentation

I. Introduction

Gastric emptying, motility, and intestinal transit are essential aspects of gastrointestinal (GI) function [1]. Impairment of such responses may cause gastroparesis [2, 3], obesity [4], and gastroesophageal reflux diseases [5]. Understanding and diagnosis of gastric disorders require direct and accurate assessment of gastric emptying and motility. In this regard, current tools are mostly based on radioactive imaging [6, 7] or measurements through invasive intubation [8-12], which are unsafe for repeated measurements, technically cumbersome, and/or physiologically confounding. In contrast, magnetic resonance imaging (MRI) is emerging as a likely more favorable alternative for imaging GI anatomy and function with excellent soft-tissue contrast and high spatial resolution [13]. Initial applications of gastric MRI in humans have demonstrated its unique potential for comprehensive assessment of gastric emptying [7, 14], intra-gastric distribution [15], and antral and duodenal motility [16, 17], to name a few.

Despite its increasing applications in humans [13, 18-20], gastric MRI has rarely been applied to small animals [21-24]. However, fundamental knowledge about the GI physiology and pathology often results from animal studies, and new therapeutics are typically tested first in animal models (especially rodents) before clinical trials. It is thus of interest to establish gastric MRI in rodents for basic science and preclinical studies. Doing so would also pave the way to combine MRI with a rich set of techniques that are more readily applicable to rodents than humans for mechanistic insights into GI physiology, diseases, and therapeutics. For example, one of such avenues is to combine gastric MRI with electrophysiology [25, 26], hormone [27-29], and behavioral [30] essays to evaluate the emerging bioelectric therapeutics [25, 31-33]. Nevertheless, gastric MRI is still premature for animal studies, and it is lack of standardized routines for either image acquisition or analysis.

Establishing gastric MRI in rodents is not simply a backward translation from humans. There are practical and technical challenges unique to rodents. In vivo gastric imaging is generally more difficult in rodents given their much faster gastric motility [34]. Besides, rodents, unlike humans, are not compliant to self-directed food ingestion or breath holding, both of which are critical requirements for gastric MRI in humans, thus calling for adaptation of the MRI protocols to avoid otherwise poorly controlled experiments and severe motion artifacts. The complex GI geometry and inhomogeneous lumen contrast also place challenges to image processing [19]. To date, gastric MRI analysis relies on manual and labor-intensive efforts, while being potentially subjective and inaccurate. Automated image

processing is piecemeal for gastric MRI, severely limiting its throughput, dissemination, and application in both humans and animals [35].

The goal of this study was to overcome the above limitations to establish gastric MRI in rats as a robust, standardized, and quantitative imaging technique. Specifically, we introduced an animal feeding protocol to train rats for self-direct consumption of a Gadolinium-labeled test meal right before MRI. This protocol served to control food ingestion for consistency across animals, and to enhance GI contrast in T1-weighted and high-field MRI. With the enhanced contrast/signal to noise ratios, we optimized the MRI acquisition to assess either gastric emptying or motility with relatively high spatial or temporal resolution, respectively. We further developed computer-assisted image processing pipelines to streamline the analysis of gastric MRI data for quantitative and objective assessment of gastric anatomy, emptying and motility, etc.

II. Materials and Methods

A. Animal Protocol

Eleven rats (Sprague-Dawley, male, adult, 229-330g) were studied according to a protocol approved by the Institutional Animal Care and Use Committee at Purdue University. The animals were housed individually in a ventilated cage with lifted stainless steel wire floor, and maintained on a 12:12h light-dark cycle (lights on at 6AM and lights off at 6PM).

Each animal was trained to consume a fixed quantity of palatable dietgel (DietGel Recovery, ClearH2O, ME, USA). The diet training took about 7 days. In the first 2 days, the animal was supplied with both regular rat chow and ~10g dietgel (the dietgel was put in a dish in the cage at 11AM) to accustom itself to the dietgel. In the following days, the animal was fasted for 18 hours (5PM to 11AM) and then was fed with the dietgel only at 11AM. The animal was given 30 minutes to consume 10g dietgel; then regular meals were supplied to the animal afterwards regardless of whether it finished the dietgel or not. After the diet training (~2 to 3 repetitions), each animal was able to naturally consume the dietgel following overnight food restriction.

On the day for gastric MRI, each animal was given a test meal with a mixture of the dietgel and an MRI contrast agent – Gadolinium (Gd). Specifically, 10g dietgel was liquefied by double-boiling in the warm water, and then it was mixed with 22.4 mg powder-form of Gd-DTPA (#381667, Sigma Aldrich, St. Louis, USA) to obtain a 4mM-quivalent solution. The liquefied dietgel was cooled to the room temperature to reform itself to the gel state.

Given the over-night food restriction, every animal was able to consume the Gd-labeled test meal in several minutes. Then, it was anesthetized with 4% Isoflurane mixed with oxygen at a flow rate of 500ml/min for 5 minutes, and it was then placed on a water-heated cradle in prone position. On the cradle, the animal received a subcutaneous (SC) bolus injection of 0.01mg/kg dexmedetomidine solution (0.05mg/ml, Zoetis, NJ, USA). About five minutes later, 0.3-0.5% isoflurane mixed with oxygen at a flow rate of 500ml/min was continuously delivered through a nose cone. About fifteen minutes after the bolus, continuous SC infusion of dexmedetomidine at 0.03mg/kg/hour was administered. An MRI-compatible system (SA

Instruments Inc., Stony Brook, NY, USA) was used to monitor the animal's respiration, cardiac pulsation, and body temperature to ensure a stable physiological state throughout the experiment.

B. Gastric MRI

The animals were scanned in a 7-tesla horizontal-bore small-animal MRI system (BioSpec 70/30; Bruker Instruments, Billerica, USA) equipped with a gradient insert (maximum gradient: 200mT/m; maximum slew rate: 640T/m/s), and a volume transmit/receive 1H RF coil (86 mm inner-diameter).

The MRI protocol started with an abdominal localizer to acquire T2-weighted scout images to reveal the long axis of the stomach (Fig. 1B). Along this long axis, two sets of T1-weighted coronal images were acquired using a two-dimensional Fast Low Angle Shot gradient echo (FLASH) sequence: one for assessing gastric volume with higher spatial resolution and larger spatial coverage (herein referred to as the "volumetric" scan, Fig. 1C), and the other for assessing gastric motility with higher temporal resolution and more targeted spatial coverage (referred to as the "fast" scan, Fig. 1D). As the Gd-labeled test meal initially filled the stomach and progressively entered the intestines, the GI volumes were rendered with much higher T1-weighted intensities, providing greatly enhanced contrast against other visceral organs.

The volumetric and fast scans were repeated in an interleaved manner (Fig. 1A) for a total of four hours. The volumetric scans were acquired with repetition time (TR) = 124.131 ms, echo time (TE) = 1.364 ms, flip angle (FA) = 90°, 30 oblique slices, slice thickness = 1 mm, FOV = 60 × 60 mm^2, in-plane resolution= 0.23 × 0.23 mm^2, 4 averages, and no repetition. The fast scans were acquired with TR/TE = 11.784/1.09ms, FA = 25°, four oblique slices, slice thickness = 1.5mm, FOV = 60 × 60 mm^2, in-plane resolution 0.47 × 0.47 mm^2, no averaging, and 150 repetitions. The four fast scan slices were positioned and adjusted to cover the antrum, pylorus and duodenum based on the immediately preceding volumetric images to account for the stomach displacement during gastric emptying. To mitigate motion artifacts, both volumetric and fast scans were respiration-gated such that images were acquired during end-expiratory periods while the chest volume stayed roughly unchanged. With the respiratory gating, the volumetric scan took about 4 minutes; the fast scan took ~2 seconds per repetition and lasted about 6 min for 150 repetitions.

C. Assessment of gastric volume, compartments, and emptying

The stomach volume was assessed both as an entire quantity and by compartments approximately every 15 mins for 4 hours. As illustrated in Fig. 2, the volumetric images were processed using a customized and automatic pipeline in Matlab (Mathworks, Massachusetts, USA) to segment the contrast-enhanced lumen volume of the GI tract.

First, a 3D fuzzy c-means clustering algorithm (fuzziness: 2.2) [36] was applied to the unprocessed images (Fig. 2A) to initially partition all voxels into two clusters: the higher-intensity Gd-labeled meal and the lower-intensity tissues (Fig. 2B). The former yielded an initial segmentation of the GI tract filled with the meal. To refine the segmentation, a localized region-based active contour segmentation algorithm [37] wasfurther applied to

each slice to correct for the heterogeneity in lumen intensities and to smooth the contour (Fig. 2C). Briefly, the algorithm operated upon a rectangular window (15-by-15 pixels) sliding across each slice; the segmentation was optimized separately for each instance of the sliding window by using the gradient-descend method to minimize the intensity inhomogeneity in both the segmented and non-segmented regions while regularizing the arc length of the contour of the segmented regions. It is important to note that some voxels outside the GI tract might be mistakenly included in the above segmentation. These included the voxels in large veins with much shortened T1 and those in the renal medulla due to systemic Gd absorption roughly 2 hours after the start of the experiment. However, such spurious voxels were identified and excluded from the GI segmentation.

Following the segmentation, the GI was divided into two compartments (the stomach and the intestines) based on an automatic image analysis. Specifically, the segmented volume (Fig. 2C) was eroded with a disk (using a Matlab function imerode with a kernel size of 7 pixels) to disconnect the stomach and the intestines at the pylorus. After identifying the stomach and the intestines, the eroded segmentation was dilated with the same disk (using a Matlab function imdilate) to restore its original size, yielding separate stomach and intestinal segmentations (Fig. 2D). The segmented stomach volume was further sub-divided into the forestomach, the corpus, and the antrum [38]. Specifically, the forestomach and the corpus were separated by the limiting ridge, while the corpus and the antrum were separated by a line connecting the angular incisure with a point located at the highest convexity on the greater curvature of the distal stomach. To define such morphological landmarks, all the voxels inside the stomach were projected onto a planar shadow through maximum intensity projection (MIP) (Fig. 2E). A 2-D mask of the stomach contour was extracted from non-zero pixels in the MIP of the stomach (Fig. 2F). Based on this mask, a convex hull of the stomach mask was identified by first using the Matlab function (bwconvhull), followed by subtraction of the stomach mask. This resulted in the concave region of the stomach mask. One set of eight extrema points was calculated for the concave region, and another set of eight extrema points was obtained for the entire stomach mask. These were calculated using the Matlab function (regionprops with option ‘Extrema’). The bottom-right and the bottom-left extrema points of the concave region were considered to be the upper-endpoint of the limiting ridge and the angular incisure, respectively. Similarly, the bottom-right and bottom-left extrema points of the stomach mask corresponded to the lower-endpoint of the limiting ridge and the landmark on the greater curvature of the distal stomach, respectively. The bottom-right point from each region was connected and represented the limiting ridge. Similarly, the bottom-left point from each region was connected. These connections separated the stomach into the forestomach, the corpus, and the antrum (Fig. 2F, red dotted line, blue dotted line). Such compartment-wise masks were further used to partition the originally segmented stomach into 3 different compartments for all slices (i.e. forestomach, corpus and antrum, Fig. 2G, 2H).

The volume of the segmented GI was quantified as a whole and by regions. This provided the imaging-based measurements for the GI volume, the intestinal volume, the stomach volume, and the volumes of different compartments of the stomach (i.e. the forestomach, the corpus, and the antrum). The volumetric MRI scans at different times were segmented, quantified separately, and then normalized as the ratios over the total GI volume at time 0.

This allowed us to observe the relative volume change over time for each animal, while the normalization additionally accounted for the varying amount of the meal intake for different animals. The time series of gastric volumes were resampled at 15-min intervals for every animal and then averaged across animals to characterize gastric emptying in the group level.

D. Assessment of gastric motility

Similarly, the images from the fast scans were processed by using a custom-built pipeline in Matlab (Fig. 3). First, the fast scans were aligned to their immediately previous volumetric scans with rigid body transformation. Next, a rectangular region of interest (ROI) was set up to cover the antrum on every slice of the fast scans (Fig. 3A). Within this ROI, high-intensity voxels (i.e. the Gd-labeled meal) were segmented by using an automatic clustering-based image thresholding method as described elsewhere [39] (Fig. 3B). To obtain the antral motility representation from the peristaltic wave (Fig. 3C), we implemented an algorithm similar to one previously developed for human antral imaging [40]. Specifically, perpendicular to the antral axis, cross-sectional planes were defined at different positions at the axis. The segmented voxels within each cross section were summed over all slices to quantify the cross-sectional area along such axis. As a result, the antral volume was expressed as a line profile, where each intensity value represented the antral area in a cross section at the specific position along the axis. The line profiles were then stacked over times and graphed (herein referred to as the antral motility representation) (Fig. 3D), in which the horizontal axis represents time and the vertical axis represents the distance from the proximal antral to the distal antrum. The antrum contraction terminated at the pylorus opening, where there was no (or at least minimal) contractile activity represented by the cross-sectional area change. The antral contraction frequency, velocity and amplitude were obtained from the antral motility representation. The middle of the peristaltic pathway was automatically determined, which resulted in a horizontal line that was passed through this location. The intensity profile was then sampled along the line and plotted as shown in Fig. 3E. The sampled signal intensity represented the temporal change of the cross-sectional areas over time. The peaks (marked as *) and the valleys (marked as o) of the time series were automatically detected, which corresponded to the maximal and minimal size of the antrum corresponding to the antral distension and contraction, respectively. The percentage occlusion of the antrum (herein referred to the contraction amplitude) was obtained by calculating the ratio of the peak-valley difference over the peak size. This was repeated and then averaged across all the peak-valley pairs on the motility representation, yielding an average percentage occlusion of the antrum. To estimate the frequency of the antral contraction, the Fourier transformation was applied to the time series of the antral contraction, followed by the peak detection in the magnitude of the frequency spectrum. For computing the propagating velocity of the antral peristaltic wave, two intensity profiles were sampled at two voxels above and below the middle of the peristaltic pathway. The distance between the two lines was 5 voxels, which corresponded to 2.344 mm with our imaging protocol. The valleys on each sampled line were computed, and plotted as the white dots on the motility diagram (Fig. 3F). Therefore, the gradient (Δdistance/Δtime) was computed by calculating the distance and time difference between two paired white dots, reporting the propagating velocity of the peristaltic wave.

III. RESULTS

A. Contrast-enhanced gastric MRI

After a 7-day diet training followed by an 18-hour fast, each of the eleven animals was able to naturally consume a Gd-labeled test meal (Mean±S.D=6.90±1.33g; 5.43±1.05ml). Immediately after the meal, the animal was sedated and scanned with MRI for 4 hours (Fig. 1). None of the animals showed any abnormal behavior or syndrome either during the diet training or after recovery from MRI. Repeated measurement was plausible on the same animal. In T1-weighted abdominal MRI, the test meal showed much higher intensity than surrounding tissues (Fig. 1C). The contrast enhancement was pronounced during the entire experiment. As the ingested meal initially filled the stomach and then the intestines, it delineated the gastric lumen and revealed the gastric emptying and intestinal filling with high contrast and resolution for robust and quantitative analysis.

B. Gastric emptying

Fig. 4A shows the high-definition 3D-rendered gastric volumes for different compartments automatically segmented from the MRI images (as illustrated in Fig. 2). The regional volumes in the stomach and the intestines were normalized against the total GI volume at time 0 within each animal, and then averaged across animals. At time 0, the stomach (Fig. 4C) and intestinal volumes (Fig. 4D) were 84.81±1.92% and 15.19±1.92%, respectively (n=11), summing up to 1 for the total GI volume. The stomach volume progressively decreased due to gastric emptying (Fig. 4C), which was notably faster during the first 30 minutes than during the rest of the experiment. Along with this observation, the intestinal volume increased as the labeled meal filled the intestines, especially during the first 30 minutes (Fig. 4D). Afterwards, the intestinal volume decreased due to intestinal absorption from 30 to 60 minutes, and stayed roughly unchanged from 60-240 minutes, reflecting a balance between intestinal filling and absorption. Note that the total GI volume increased during the first 30 minutes (Fig. 4B). This observation was likely attributed to gastric secretion. The total GI volume monotonically decreased from 30 to 240 minutes (Fig. 4B), suggesting that there was a higher rate of gastric absorption than secretion during this period. After four hours in a sedated condition, the stomach volume decreased by 27% on average. This was mostly attributable to the progressive emptying of the forestomach (Fig. 4E), whereas the corpus and the antrum had relatively minor volume changes (Fig. 4F and 4G). Quantitatively, the forestomach volume decreased from 64.20±3.43% to 47.60±3.71% (Fig. 4E); the corpus volume decreased from 17.84±1.85% to 12.33±1.828% (Fig. 4F); and the antral volume decreased from 5.34±0.62% to 4.07±0.61% (Fig. 4G). The volume and morphological changes of the stomach and its compartments were apparent in multi-slice MRI images, showing high-resolution and high-contrast depiction of the lumen content in the GI tracts (Fig. 5). See supplementary video 1 for a fast-forwarded movie of gastric MRI over a 4-hour period of gastric emptying (supplementary video 1: Example semi-coronal view of the GI tract from the 2D multi-slice volumetric scans for four hours).

C. Antral motility

When sampled with high temporal resolution around 2 seconds, the contrast-enhanced gastric MRI captured the gastric motility as a wave of antral contraction propagating along

the long axis of the antrum (Supplementary video 2: Fast scans of the antrum with four slices in 20 minutes reveal the temporal progression of the peristaltic wave; The frame rate was set to be 8 frames per second). As shown in Fig. 3, this antral peristaltic wave could be quantitatively characterized to accurately measure the frequency, amplitude, and velocity of the antral contraction. Averaged across animals, the frequency and velocity of antral contraction as well as the amplitude of antral occlusion, were 6.34±0.07 contractions per minute, 0.67 ±0.02 mm/s and 30.58±1.03%, respectively.

We also evaluated the correlation between antral motility and stomach emptying across animals. As shown in Fig. 6, no correlation was observed between stomach emptying and antral contraction frequency (r=0.0056) or amplitude (r=0.0555), whereas there was a weak correlation with the contraction velocity (r = 0.2709).

D. Intestinal absorption

Along with our observation that the total GI volume decreased during the period from 30 to 240 minutes, there was a progressively emerging signal intensity enhancement in the renal medulla roughly 2 hours after the start of the experiment (Fig. 7). This was likely due to the systemic accumulation of circulating Gd absorbed from the mucosa of the intestinal walls. The kinetics of how the kidney handled the systemically circulating gadolinium provided an indirect measurement of the intestinal absorption of nutrients.

IV. Discussion

A. Highly benign and effective animal feeding protocol

In this study, the animals were trained for one week to spontaneously consume a post-fast meal laced with trace amounts of gadolinium [the concentration was adapted from human feeding protocols [24]]. This allowed us to define gastrointestinal organs with high-resolution and high-contrast MRI. Although free gadolinium ion (Gd^{3+}) is a toxic lanthanide heavy metal, the compound is considered to be biologically safe when combined with other chelates such as DTPA and DOTA [41]. Adverse effects of oral or intravenous administration of gadolinium-based contrast agent were only recently found in patients with severe renal impairments [42]. This was likely due to impaired clearance of gadolinium by the kidney, which led to tissue accumulation of dissociated Gd^{3+}. A potential alternative to Gd-DTPA is Gd-DOTA, which is a more stable contrast agent in acidic gastric environment. Additionally, Gd-DOTA would not be easily absorbed by the GI tract, thus reducing the amount of systemically circulating gadolinium that kidneys need to handle [43].

A notable advantage of this protocol is that it bypasses the need of oral gavage. Oral gavaging introduces a major non-physiological simplification and considerable stress to the animal. Additionally, it may alter the physiological gut-brain coordination with normal food ingestion, in which the natural interaction between dietary exposure and oral mucosa is necessary for proper cognitive and sensory processing as well as gastric accommodation reflexes [44, 45].

B. Gastric emptying and secretion

The ingestion volume, the secretion volume, and the volume that empties out of the stomach account for the total stomach volume change. This differs for the intestine, where the volume that transits from the stomach and the volume of chyme that is absorbed through the intestinal mucosa account for the change in the intestinal volume. Given the fact that the animal did not ingest any additional food during MRI scans, the change in the gastric volume was strictly determined by the decrease throughout the emptying process and the increase in secretion volume.

Our finding that the gastric emptying rate was largely attributed to the emptying rate of the forestomach is consistent with previous findings that emptying rates were higher in the forestomach than in the glandular stomach in rats [46, 47]. Therefore, the MRI-enabled compartment-wise analysis offers the sensitivity and specificity in detecting regional differences in emptying within the stomach, and may potentially be useful for examining different pathological disorders (i.e. gastroparesis).

In this study, we could not differentiate the remaining meal and the gastric secretion in the stomach, because the latter also appeared with high contrast in MRI. One way to separate meal and gastric juice may be based on in vitro calibration of either the T1-weighted signal intensity [7], T1 [48, 49], or T2 value [15] for these two substances, for example by diluting the test meal with different amounts of hydrochloric acid to simulate the meal-juice mixture in vivo. This strategy assumes a homogeneous mixture of the meal, gastric juice and the contrast agent, and typically requires the test meal to be in the liquid state. Such assumption or requirement was not met in this study since our test meal was a viscous semi-solid dietgel that appeared heterogeneous in the gastric lumen with small intra-gastric air cavities. Moreover, the dilution and mixture of a viscous test meal with secretion juice is slow and uneven in the stomach, mostly occurring at the wall of the lumen [15]. Future methodological development is much desired to accurately assess gastric secretion for various types of test meal.

C. Confounding effect of anesthetic agent

One of the major limitations of doing gastric MRI in animals is the need of anesthetics for restraining them from body movement. As a result, the choice of anesthetic(s) is critical, given that different anesthetics alter the GI functions differently. Here, we chose to use a combination of dexmedetomidine and low dose of isoflurane. The reasoning behind this choice is twofold; although it has been reported that dexmedetomidine delays gastric emptying, the effect is weak compared to saline placebo [50]. In contrast, using isoflurane alone would significantly impact the activity of the gut by a reduction of 50% in GI transits [51]. Further, it is also critical to understand the biochemical and bioelectrical signaling processes in between the enteric and central nervous systems. In this regard, MRI serves as a versatile imaging tool to investigate brain functions (i.e. functional MRI), especially because there is an emerging interest in examining the functional network in the rodent brain [52, 53]. A common anesthetic protocol that could serve both needs is advantageous because it could potentially be used for imaging both the GI tract and the rodent brain. As such, we adopted and adapted the anesthetic protocol from [53] for neural imaging in rats. This has

previously been shown to better preserve the functional activities in rodent's central nervous system (CNS) under longitudinal experiments [54], as compared to using isoflurane alone. By combining the use of these two anesthetics, our dosage for each of them was well below what has been reported in the earlier studies. However, we do not rule out the possibility that the gastric functions are (at least minimally) affected by the anesthetics. It might be possible to adopt the animal protocol developed in animal brain imaging [55, 56] to train animals to stay still during gastric MRI in future studies.

V. Conclusion

Here, we present a robust and effective contrast-enhanced MRI method to image and characterize gastric emptying and motility in rats. This method includes animal training and MRI imaging protocols as well as image analysis pipelines. Our results demonstrate the promise of using gastric MRI to non-invasively and quantitatively assess the emptying of the stomach and its compartments. It also allows quantitative evaluation of the antral motility in terms of the frequency, amplitude, and velocity of the antral peristaltic wave. This technique not only allows for repeated assessment within animals, but also shows consistent assessment across animals. It is thus well-suited for basic-science and preclinical studies of gastric physiology and diseases.

Supplementary Material

Refer to Web version on PubMed Central for supplementary material.

Acknowledgments

This work was supported in part by NIH SPARC 1OT2TR001965 and Purdue University. Authors have no conflict of interest.

REFERENCES

[1]. Thomas JE, "Mechanics and regulation of gastric emptying," Physiological reviews, vol. 37, no. 4, pp. 453–474, 1957. [PubMed: 13484472]

[2]. Parkman HP et al., "American Gastroenterological Association technical review on the diagnosis and treatment of gastroparesis," Gastroenterology, vol. 127, no. 5, pp. 1592–1622, 11, 2004. [PubMed: 15521026]

[3]. Patrick A and Epstein O, "Review article: gastroparesis," Alimentary pharmacology & therapeutics, vol. 27, no. 9, pp. 724–740, 2008. [PubMed: 18248660]

[4]. Woods S and Seeley R, "Understanding the physiology of obesity: review of recent developments in obesity research," International Journal of Obesity, vol. 26, no. S4, p. S8, 2002. [PubMed: 12457292]

[5]. El–Serag HB, "Time trends of gastroesophageal reflux disease: a systematic review," Clinical Gastroenterology and Hepatology, vol. 5, no. 1, pp. 17–26, 2007. [PubMed: 17142109]

[6]. Couturier O et al., "Gastric scintigraphy with a liquid–solid radiolabelled meal: performances of solid and liquid parameters," Nuclear medicine communications, vol. 25, no. 11, pp. 1143–1150, 2004. [PubMed: 15577595]

[7]. Feinle C et al., "Scintigraphic validation of a magnetic resonance imaging method to study gastric emptying of a solid meal in humans," Gut, vol. 44, no. 1, pp. 106–111, 1999. [PubMed: 9862835]

[8]. De Schepper H et al., "Assessment of gastric accommodation: overview and evaluation of current methods," Neurogastroenterology & Motility, vol. 16, no. 3, pp. 275–285, 2004. [PubMed: 15198649]

[9]. Schwizer W et al., "Measurement of gastric emptying and gastric motility by magnetic resonance imaging (MRI)," Digestive diseases and sciences, vol. 39, no. 12, pp. 101S–103S, 1994. [PubMed: 7995199]

[10]. Azpiroz F and Malagelada J-R, "Gastric Tone Measured by an Electronic Barostat in Health arid Postsurgical Gastroparesis," Gastroenterology, vol. 92, no. 4, pp. 934–943, 1987. [PubMed: 3556999]

[11]. de Zwart IM et al., "Gastric accommodation and motility are influenced by the barostat device: assessment with magnetic resonance imaging," American Journal of Physiology-Gastrointestinal and Liver Physiology, vol. 292, no. 1, pp. G208–G214, 2007. [PubMed: 16891299]

[12]. Björnsson E and Abrahamsson H, "Interdigestive gastroduodenal manometry in humans. Indication of duodenal phase III as a retroperistaltic pump," Acta Physiologica, vol. 153, no. 3, pp. 221–230, 1995.

[13]. Schwizer W et al., "Magnetic resonance imaging for the assessment of gastrointestinal function," Scandinavian journal of gastroenterology, vol. 41, no. 1, pp. 1245–1260, 2006. [PubMed: 17060117]

[14]. Schwizer W et al., "Measurement of gastric emptying by magnetic resonance imaging in humans," Gastroenterology, vol. 103, no. 2, pp. 369–376, 1992. [PubMed: 1634055]

[15]. Marciani L et al., “Effect of meal viscosity and nutrients on satiety , intragastric dilution , and emptying assessed by MRI,” pp. 1227–1233, 2001.

[16]. Treier R et al., "Gastric motor function and emptying in the right decubitus and seated body position as assessed by magnetic resonance imaging," Journal of Magnetic Resonance Imaging, vol. 23, no. 3, pp. 331–338, 2006. [PubMed: 16463302]

[17]. Baba S et al., "Assessment of gastric motor function by cine magnetic resonance imaging," Journal of Gastroenterology and Hepatology (Australia), vol. 24, no. 8, pp. 1401–1406, 2009.

[18]. Schwizer W et al., "Non-invasive investigation of gastrointestinal functions with magnetic resonance imaging: towards an “ideal” investigation of gastrointestinal function," Gut, vol. 52, no. suppl 4, pp. iv34–iv39, 2003. [PubMed: 12746267]

[19]. Marciani L, "Assessment of gastrointestinal motor functions by MRI: A comprehensive review," Neurogastroenterology and Motility, vol. 23, no. 5, pp. 399–407, 2011. [PubMed: 21276139]

[20]. Khalaf A et al., "Magnetic resonance imaging biomarkers of gastrointestinal motor function and fluid distribution," World journal of gastrointestinal pathophysiology, vol. 6, no. 4, pp. 140–9, 2015. [PubMed: 26600972]

[21]. Ailiani AC et al., "Quantitative analysis of peristaltic and segmental motion in vivo in the rat small intestine using dynamic MRI," Magnetic Resonance in Medicine, vol. 62, no. 1, pp. 116–126, 2009. [PubMed: 19353667]

[22]. Ailiani AC et al., "Quantifying the effects of inactin vs Isoflurane anesthesia on gastrointestinal motility in rats using dynamic magnetic resonance imaging and spatio-temporal maps," Neurogastroenterology and Motility, vol. 26, no. 10, pp. 1477–1486, 2014. [PubMed: 25257924]

[23]. Wan X et al., "Sources of heterogeneous contrast enhancement in the gastrointestinal tract," Magnetic resonance imaging, vol. 12, no. 7, pp. 1009–1012, 1994. [PubMed: 7997087]

[24]. Wan X et al., "MRI evaluation of potential gastrointestinal contrast media," Magnetic resonance imaging, vol. 13, no. 2, pp. 215–218, 1995. [PubMed: 7739362]

[25]. Liu J et al., "Vagal afferent is involved in short-pulse gastric electrical stimulation in rats," Digestive Diseases and Sciences, vol. 49, no. 5, pp. 729–737, 2004. [PubMed: 15259491]

[26]. Song G-Q et al., "Gastric electrical stimulation with long pulses in humans and animals: can data obtained in animals be replicated in humans?," Neuromodulation : journal of the International Neuromodulation Society, vol. 13, no. 2, pp. 87–92, 2010. [PubMed: 21992779]

[27]. Masuda Y et al., "Ghrelin stimulates gastric acid secretion and motility in rats," Biochemical and biophysical research communications, vol. 276, no. 3, pp. 905–908, 2000. [PubMed: 11027567]

[28]. Murray CD et al., "Ghrelin enhances gastric emptying in diabetic gastroparesis: a double blind, placebo controlled, crossover study," Gut, vol. 54, no. 12, pp. 1693–1698, 2005. [PubMed: 16085693]

[29]. Dockray GJ, "Gastrointestinal hormones and the dialogue between gut and brain," The Journal of physiology, vol. 592, no. 14, pp. 2927–2941, 2014. [PubMed: 24566540]

[30]. Murray S et al., "Hormonal and neural mechanisms of food reward, eating behaviour and obesity," Nature Reviews Endocrinology, vol. 10, no. 9, pp. 540–552, 2014.

[31]. Ishiguchi T et al., "Inhibitory neural pathway regulating gastric emptying in rats," Journal of the Autonomic Nervous System, vol. 79, no. 1, pp. 45–51, 2000. [PubMed: 10683505]

[32]. Krolczyk G et al., "Effects of continuous microchip (MC) vagal neuromodulation on gastrointestinal functional pathway," Journal of Physiology and Pharmacology, vol. 52, no. 4, pp. 705–715, 2001. [PubMed: 11787768]

[33]. Ataka K et al., "Obestatin inhibits motor activity in the antrum and duodenum in the fed state of conscious rats," American journal of physiology. Gastrointestinal and liver physiology, vol. 294, no. 5, pp. G1210–G1218, 2008. [PubMed: 18325980]

[34]. Jordi J et al., "Simultaneous assessment of gastric emptying and secretion in rats by a novel computed tomography-based method," American journal of physiology. Gastrointestinal and liver physiology, vol. 306, no. 3, pp. G173–82, 2014. [PubMed: 24264048]

[35]. Bharucha AE et al., "Comparison of Manual and Semi-Automated Techniques for Analyzing Gastric Volumes with MRI in Humans," Am J Physiol Gastrointest Liver Physiol, no. 1, pp. 582–587, 2014.

[36]. Bezdek JC et al., "FCM: The fuzzy c-means clustering algorithm," Computers & Geosciences, vol. 10, no. 2–3, pp. 191–203, 1984.

[37]. Lankton S and Tannenbaum A, "Localizing region-based active contours," IEEE transactions on image processing, vol. 17, no. 11, pp. 2029–2039, 2008. [PubMed: 18854247]

[38]. Willet SG and Mills JC, "Stomach organ and cell lineage differentiation: from embryogenesis to adult homeostasis," CMGH Cellular and Molecular Gastroenterology and Hepatology, vol. 2, no. 5, pp. 546–559, 2016. [PubMed: 27642625]

[39]. Otsu N, "A threshold selection method from gray-level histograms," Automatica, vol. 11, no. 285–296, pp. 23–27, 1975.

[40]. Marciani L et al., "Antral motility measurements by magnetic resonance imaging," Neurogastroenterology & Motility, vol. 13, no. 5, pp. 511–518, 2001. [PubMed: 11696113]

[41]. Caravan P et al., "Gadolinium (III) chelates as MRI contrast agents: structure, dynamics, and applications," Chemical reviews, vol. 99, no. 9, pp. 2293–2352, 1999. [PubMed: 11749483]

[42]. Rogosnitzky M and Branch S, "Gadolinium-based contrast agent toxicity: a review of known and proposed mechanisms," Biometals, vol. 29, no. 3, pp. 365–376, 2016. [PubMed: 27053146]

[43]. Schwizer W et al., "Gd-DOTA as a gastrointestinal contrast agent for gastric emptying measurements with MRI," Magnetic resonance in medicine, vol. 31, no. 4, pp. 388–393, 1994. [PubMed: 8208114]

[44]. Brown AP et al., "Stress produced by gavage administration in the rat," Journal of the American Association for Laboratory Animal Science, vol. 39, no. 1, pp. 17–21, 2000.

[45]. Bonnichsen M et al., "The welfare impact of gavaging laboratory rats," ANIMAL WELFARE-POTTERS BAR THEN WHEATHAMPSTEAD-, vol. 14, no. 3, p. 223, 2005.

[46]. Kunstyr I et al., "Investigations on the function of the rat forestomach," Laboratory animal science, vol. 26, no. 2 Pt l, pp. 166–170, 1976. [PubMed: 5626]

[47]. Gärtner K, "The forestomach of rats and mice, an effective device supporting digestive metabolism in muridae (review)," Journal of Experimental Animal Science, vol. 42, no. 1, pp. 1–20, 2002.

[48]. Sauter M et al., "Measuring the interaction of meal and gastric secretion: a combined quantitative magnetic resonance imaging and pharmacokinetic modeling approach," Neurogastroenterology & Motility, vol. 24, no. 7, p. 632, 2012. [PubMed: 22452723]

[49]. Hoad CL et al., "Measurement of gastric meal and secretion volumes using magnetic resonance imaging," Physics in Medicine & Biology, vol. 60, pp. 1367–1367, 2015. [PubMed: 25592405]

[50]. Asai T et al., "Differential effects of clonidine and dexmedetomidine on gastric emptying and gastrointestinal transit in the rat," British journal of anaesthesia, vol. 78, no. 3, pp. 301–307, 1997. [PubMed: 9135310]

[51]. Torjman MC et al., "Effects of Isoflurane on gastrointestinal motility after brief exposure in rats," International Journal of Pharmaceutics, vol. 294, no. 1–2, pp. 65–71, 2005. [PubMed: 15814231]

[52]. Lu H et al., "Rat brains also have a default mode network," Proceedings of the National Academy of Sciences, vol. 109, no. 10, pp. 3979–3984, 2012.

[53]. Hsu L-M et al., "Constituents and functional implications of the rat default mode network," Proceedings of the National Academy of Sciences, p. 201601485, 2016.

[54]. Grandjean J et al., "Optimization of anesthesia protocol for resting-state fMRI in mice based on differential effects of anesthetics on functional connectivity patterns," Neuroimage, vol. 102, pp. 838–847, 2014. [PubMed: 25175535]

[55]. Liang Z et al., "Uncovering intrinsic connectional architecture of functional networks in awake rat brain," Journal of Neuroscience, vol. 31, no. 10, pp. 3776–3783, 2011. [PubMed: 21389232]

[56]. Zhang N et al., "Mapping resting-state brain networks in conscious animals," Journal of neuroscience methods, vol. 189, no. 2, pp. 186–196, 2010. [PubMed: 20382183]

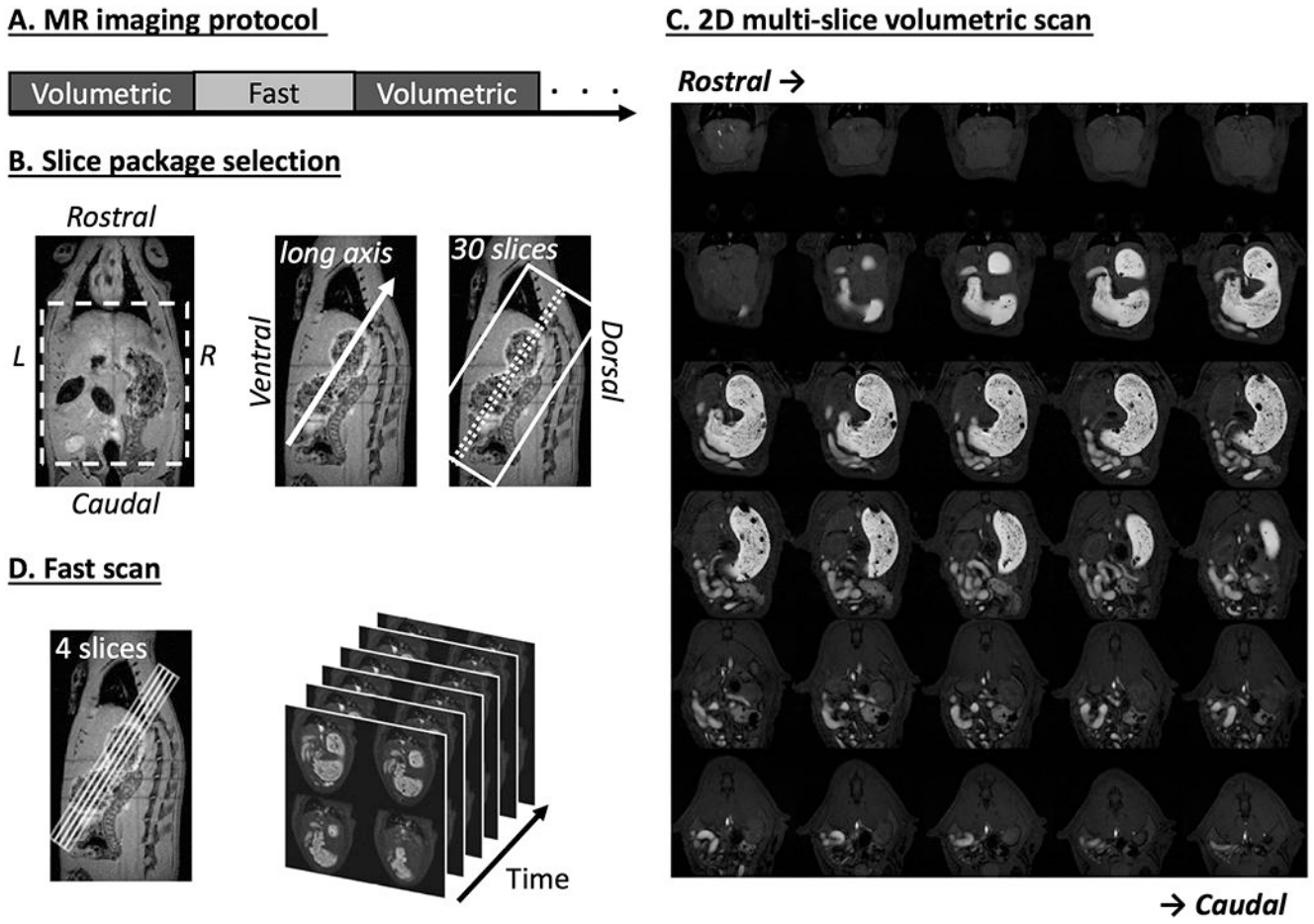

Fig. 1.

Imaging sequence and slice package selection. A. 2D multi-slice volumetric scan (denoted as “Volumetric”) and fast antral motility scan (denoted as “Fast”) were performed interleaved throughout the experiment. B. Two example T2-weighted images (left: coronal view, right: sagittal view) acquired from a multi-slice localizer sequence. An oblique 30-slice package was placed along the long axis of the stomach from the sagittal image. C. Example semi-coronal view images from the 2D multi-slice volumetric scan. D. Fast scan of the antrum with four slices. The position of the slice package was determined from images acquired from the volumetric scan.

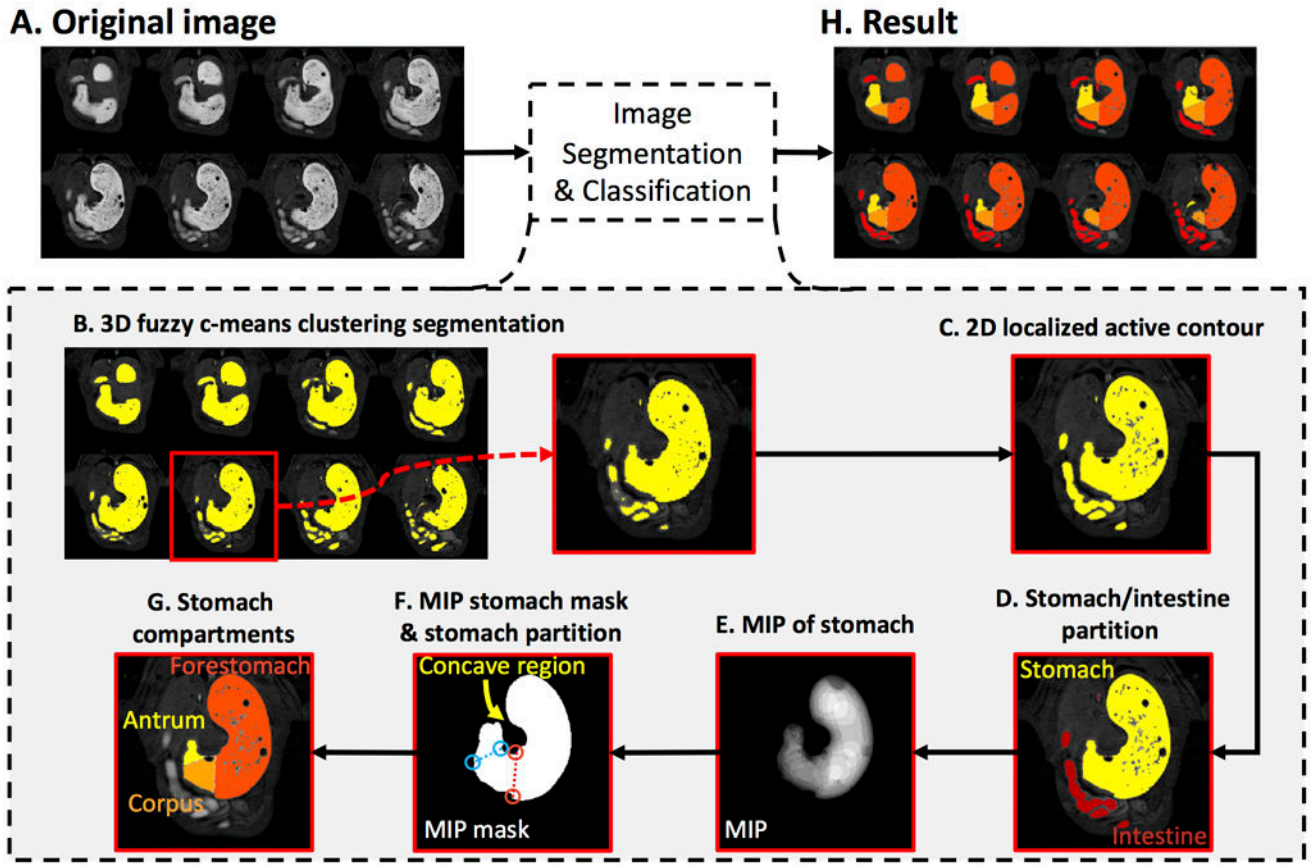

Fig. 2.

Image segmentation and classification of the GI tract. A. Contrast-enhanced gastric MRI with volumetric scans. B. Preliminary segmentation of the GI tract with 3D fuzzy c-means clustering algorithm. C. Refinement of the segmentation result with 2D localized active contour method. D. Partition of the stomach and the intestine. E. Maximum intensity projection (MIP) of the stomach. F. A stomach mask obtained from all non-zero voxels from the MIP of the stomach. The forestomach and the corpus were separated along the red dotted line, and the corpus and the antrum was separated along the blue dotted line. G. Partition of the forestomach, the corpus, and the antrum on an example slice. H. Partition of the forestomach, the corpus, the antrum, and the intestine on 8 example slices.

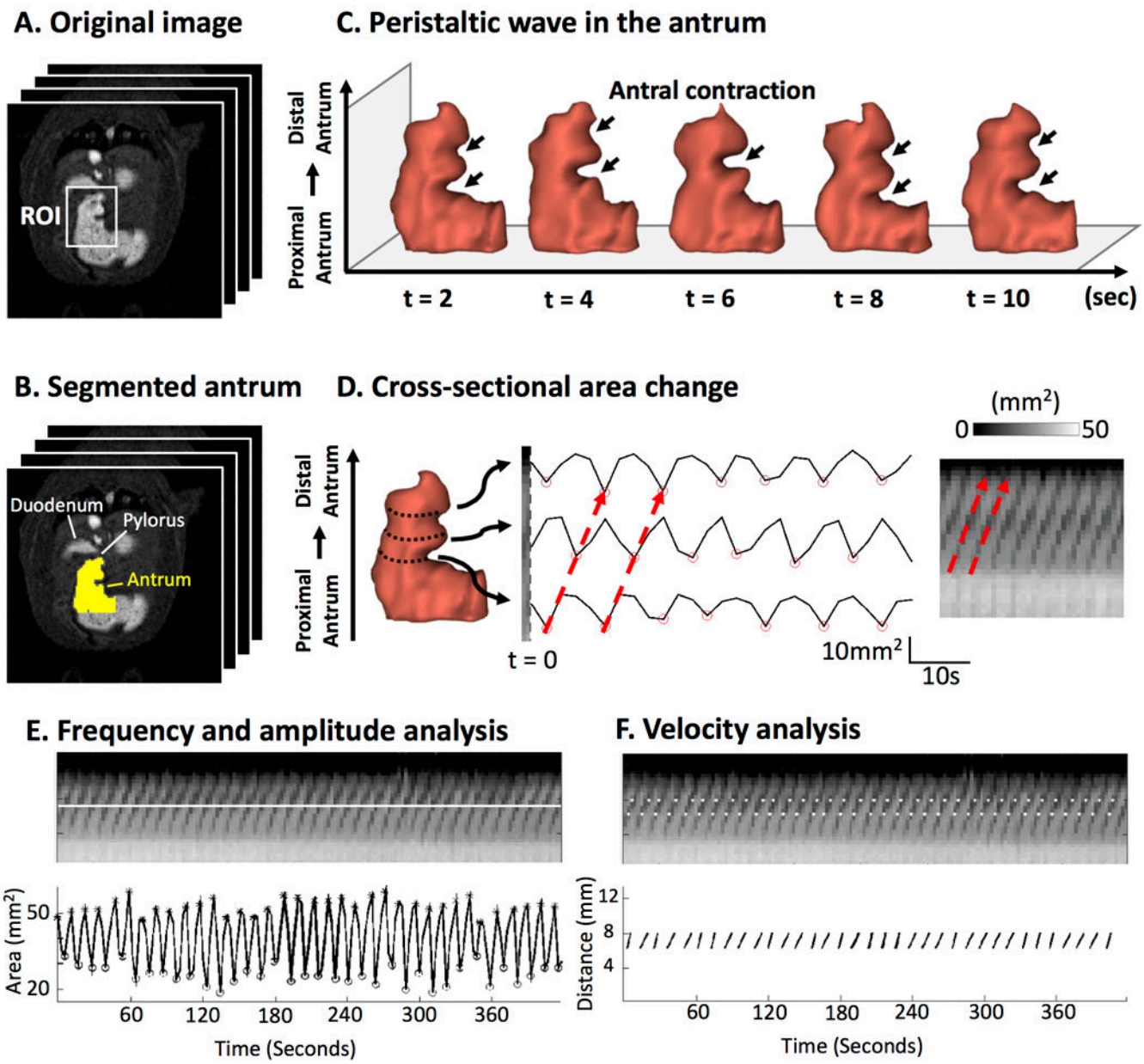

Fig. 3.

Image analysis of antral motility. A. Contrast-enhanced gastric MRI with fast sampling. B. Segmentation of the antrum. C. Temporal progression of the 3-D antral volume reveals the peristaltic wave. D. Changes in the cross-sectional area at different locations along the long axis of the antrum (from the proximal to the distal) are shown as time series or an image, both characterizing the antral motility. The red arrows mark the occurrence and progression of an antral contraction. E. The frequency and amplitude of the antral motility time series reveals the contraction frequency and amplitude. The distensions are marked with * and the contractions are marked with o. F. The spatial gradient of the phase of the motility time series reports the velocity of the peristaltic wave.

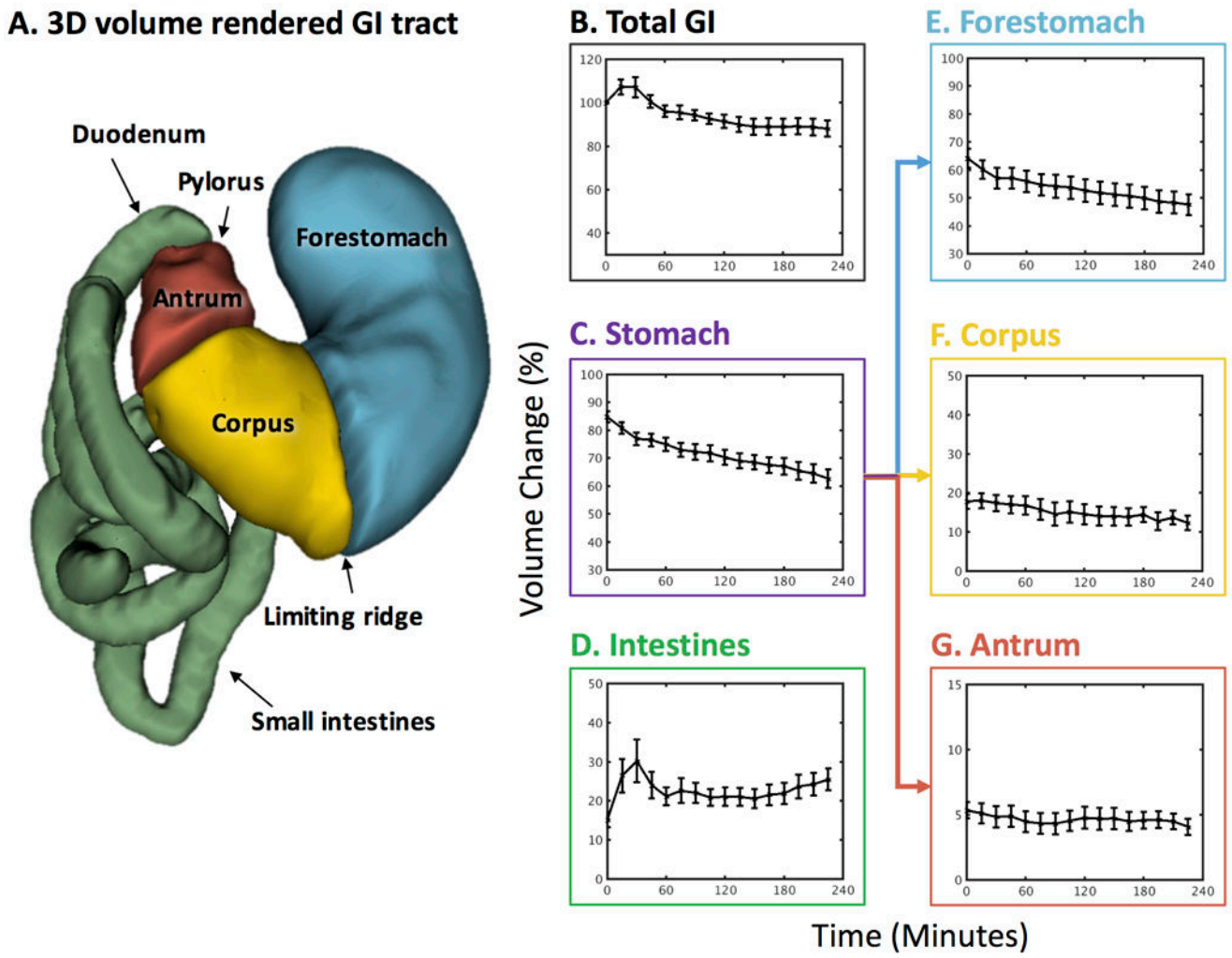

Fig. 4.

Total and compartmental gastric emptying profiles. A. 3D volume rendering of the GI tract. B. Change of the total GI volume. C. Stomach emptying profile. D. Intestinal filling profile. E. Forestomach emptying profile. F. Corpus emptying profile. G. Antrum emptying profile. All volumes were normalized against the total GI volume at time 0. Values are mean ±standard error of the mean.

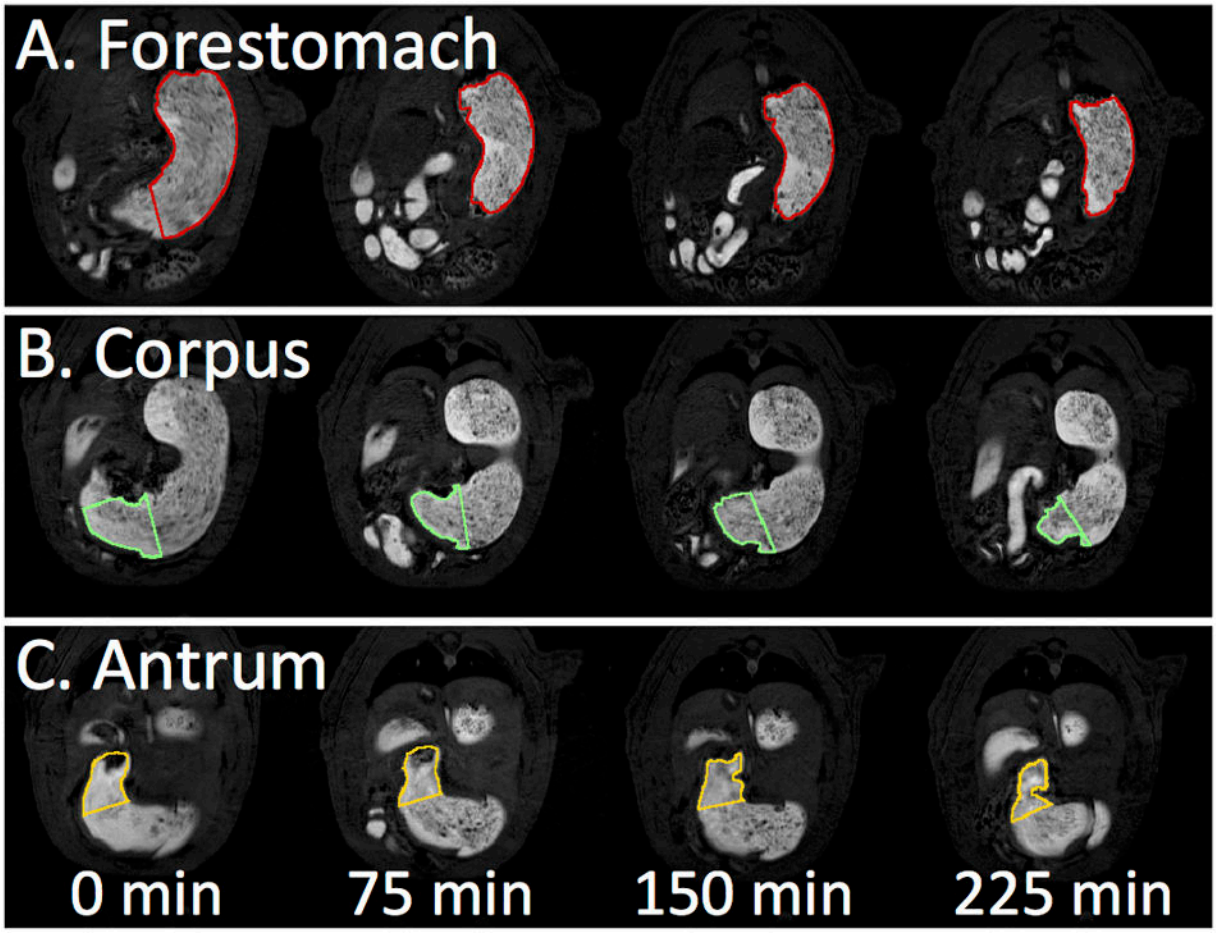

Fig. 5.

Representative slices of temporal progression of gastric emptying in different stomach compartments. A. Forestomach emptying. B. Corpus emptying. C. Antrum emptying.

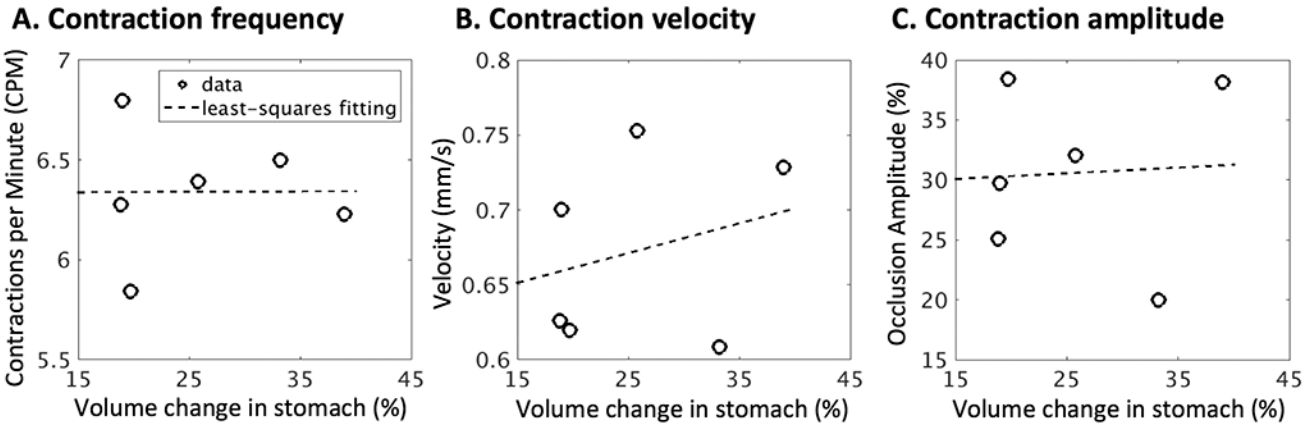

Fig. 6.

Correlates of gastric emptying rate and antral motility. A. Correlation between volume change in the stomach (%) and the antral contraction frequency (r = 0.0056). B. Correlation between volume change in the stomach (%) and the antral contraction velocity (r = 0.0555). C. Correlation between volume change in the stomach (%) and the antral contraction amplitude (r = 0.2709).

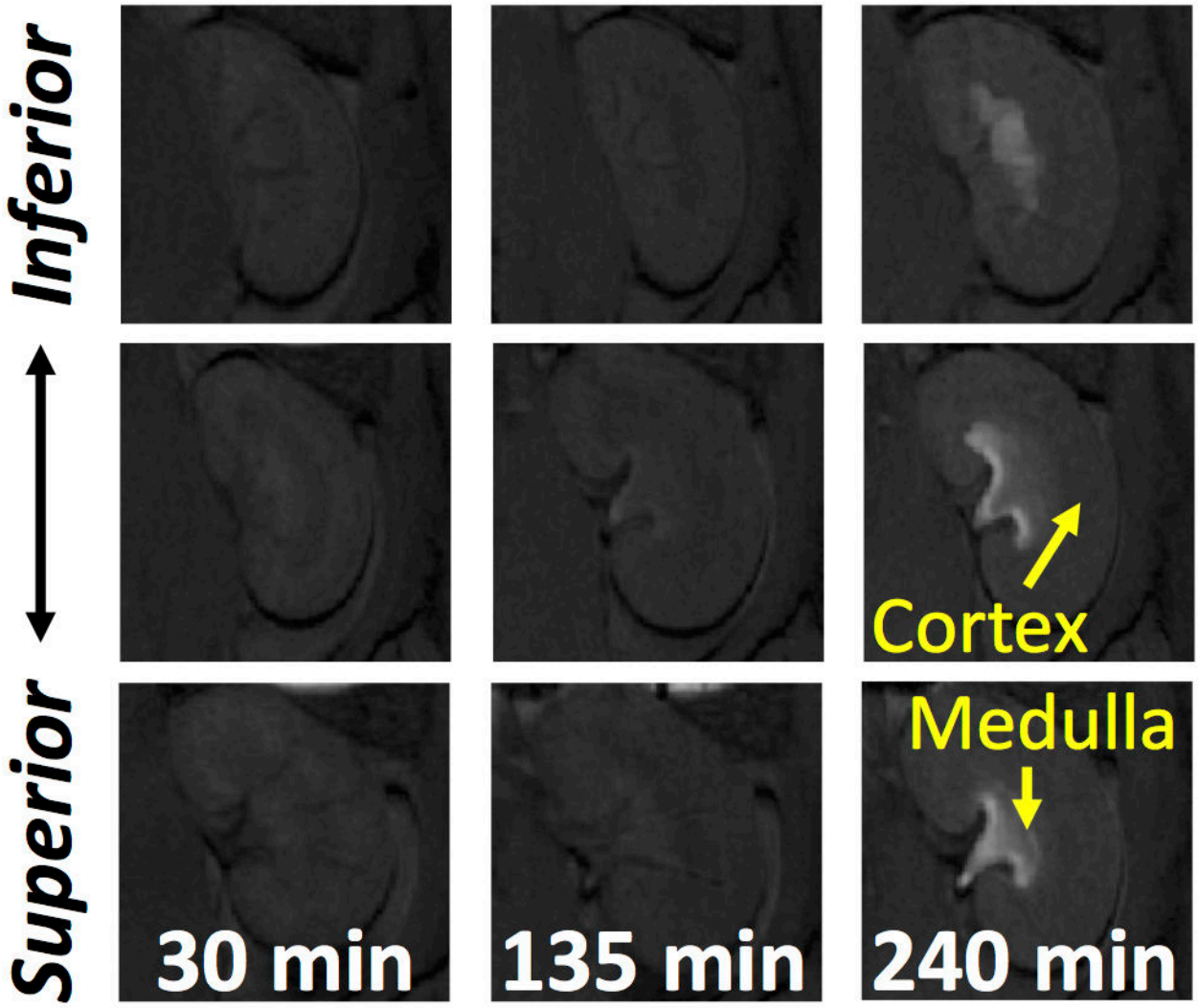

Fig. 7.

The extent of absorption of nutrients measured in terms of kidney handling of systemically circulating gadolinium. Representative slices of temporal progression of signal intensity enhancement in the renal medulla.